Microwave Absorbing Properties of $Ba_{0.6}Sr_{0.4}Fe_{12-z}Mn_zO_{19}$ (z = 0 – 3) Materials in XBand Frequencies

Yohanes Edi Gunanto[1], Eric Jobiliong[2] & Wisnu Ari Adi[3]

[1]Department of Biology Education, University of Pelita Harapan, Karawaci, Tangerang, 15811, Banten, Indonesia
[2]Department of Industrial Engineering, University of Pelita Harapan, Karawaci, Tangerang 15811, Banten, Indonesia
[3]Center for Science and Technology of Advanced Materials, National Nuclear Agency of Indonesia (BATAN), Tangerang Selatan 15314, Banten, Indonesia
E-mail: yohanes.gunanto@uph.edu

Abstract. $Ba_{0.6}Sr_{0.4}Fe_{12-z}Mn_zO_{19}$ (z = 0,1,2, and 3) were successfully synthesized by solid state reaction through a mechanical milling method. Stoichiometric quantities of analytical-grade $MnCO_3$, $BaCO_3$, Fe_2O_3, and $SrCO_3$ precursors with purity greater than 99% were mixed. It was found that the best phase composition, having an absorber with high performance, was $Ba_{0.6}Sr_{0.4}Fe_{11}MnO_{19}$. Refinement of the X-ray diffraction patterns revealed that the $Ba_{0.6}Sr_{0.4}Fe_{11}MnO_{19}$ was single-phase and had a hexagonal structure (P63/mmc). Mechanical milling of $Ba_{0.6}Sr_{0.4}Fe_{11}MnO_{19}$ powders produced particles with a mean size of ~850 nm. SEM images revealed the morphology of the particles as being aggregates of fine grains. The magnetic properties of the $Ba_{0.6}Sr_{0.4}Fe_{11}MnO_{19}$ particles showed a low coercivity and a high remanent magnetization. The $Ba_{0.6}Sr_{0.4}Fe_{11}MnO_{19}$ has certain microwave absorber properties in the frequency range of 8-14 GHz, with an absorbing peak value of -8 dB and -10 dB at frequencies of 8.5 and 12.5 GHz, respectively. The study concludes that the $Ba_{0.6}Sr_{0.4}Fe_{12}$_zMnzO_{19} that was successfully synthesized is a good candidate for use as an electromagnetic absorber material.

Keywords: *absorption; $Ba_{0.6}Sr_{0.4}Fe_{12-z}Mn_zO_{19}$; composition; magnetic; morphology; particle size.*

1 Introduction

Recently, barium-strontium hexaferrites have become the most potential candidates for electromagnetic wave absorbing materials, especially at high frequency ranges, which makes them suitable for applications such as radar absorbtion [1-3]. They have been shown to be excellent candidates for microwave absorbing materials due to their high magnetization value. However, hexaferrites, such as barium-strontium hexaferrite, have a relatively high anisotropy constant value and hence a high coercivity. Therefore, some intrinsic properties of its magnetic phase, such as the anisotropy constant, which governs the coercivity value, have to be reduced. Reduction of the anisotropy constant of

Received January 29th, 2015, 1st Revision August 26th, 2015, Accepted for publication February 2nd, 2016.
 ISSN: 2337-5760, DOI: 10.5614/j.math.fund.sci.2016.48.1.6

barium-strontium hexaferrite modification is primarily required since a substantially low coercivity and high magnetization are the most important properties required for microwave absorber applications [4-5].

By substituting Fe atoms with other atoms, one can reduce the anisotropy constant of barium strontium hexa-ferrites while their magnetization value remains high. Therefore, attempts at substitution have been made to reduce the coercive force and to increase magnetization. The application of barium-strontium hexa-ferrites in the area of electromagnetic wave absorbing materials demands proper control of homogeneity, morphology, and particle size. In addition, particle size is also well known to affect both remanence and coercivity in these materials [6-7].

The aim of this study was to synthesize $Ba_{0.6}Sr_{0.4}Fe_{12-z}Mn_zO_{19}$ (z = 0, 1, 2, and 3) materials and to investigate the phase forming, morphology, particle size, absorbing and magnetic properties exhibited by manganese substituted iron in barium-strontium hexa-ferrite structures. The focus of this study was to influence Mn substitution on the crystal structure, absorbing and magnetic properties of the barium-strontium hexaferrite.

2 Materials and Methods

$Ba_{0.6}Sr_{0.4}Fe_{12-z}Mn_zO_{19}$ (z = 0, 1, 2, and 3) was made by solid state reaction. Stoichiometric quantities of analytical-grade $BaCO_3$, $SrCO_3$, Fe_2O_3, and $MnCO_3$ precursors with a purity of greater than 99% were mixed and milled (using a high-energy milling (HEM) mixer/mill, type Spex 8000) to a 10:1 powder weight ratio for 10 hours. The sample powders were then compacted into pellets and sintered in an electric chamber furnace at 1000 °C for 10 hours to obtain crystalline materials. The sample was characterized by powder X-ray diffraction (XRD) using a Miniflex Rigaku diffractometer with CuKα radiation (λ = 1.5406 Å). The Rietveld analysis was performed by applying a GSAS program [8]. Microstructural examination and elementary analysis of the samples were conducted using scanning electron microscopy (SEM) and energy dispersive spectroscopy (EDS), respectively. The sample powders were then dispersed in distilled water and evaluated using a Helos simpatec particle size analyzer (PSA) for micron-sized particles and a Zetasizer Nano zeta potential analyzer for nano-sized particles. The magnetic properties were evaluated using an Oxford instrument vibrating sample magnetometer (VSM). Finally, measurement of reflection and transmission of microwaves was carried out using a vector network analyzer (VNA) with a frequency range of 300 kHz-20 GHz.

3 Results and Discussion

3.1 Synthesis $Ba_{0.6}Sr_{0.4}Fe_{12-z}Mn_zO_{19}$ (z = 0, 1, 2, and 3)

The X-ray diffraction profiles of the synthesized $Ba_{0.6}Sr_{0.4}Fe_{12-z}Mn_zO_{19}$ are shown in Figure 1, in which the respective profiles for z = 0, 1, 2, and 3 are compared.

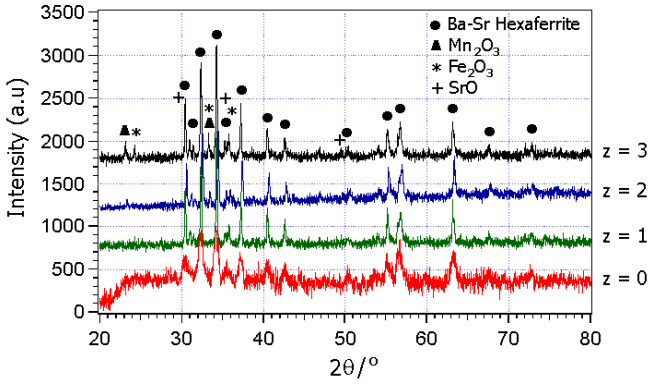

Figure 1 The XRD profiles of synthesized $Ba_{0.6}Sr_{0.4}Fe_{12-z}Mn_zO_{19}$ (z = 0, 1, 2, and 3).

It can be seen that the four diffraction profiles exhibit a pattern similar to that of $BaFe_{12}O_{19}$ phase despite a small shift in the peak positions due to the presence of partial Sr ion substitution for Ba in addition to Mn ion substitutions for Fe. However, in this case the diffraction profile for z = 1 is single-phase. Yet, the diffraction profiles for z > 1 were multi-phase and suspected to consist of Fe_2O_3 and Mn_2O_3 phases, in addition to a $BaFe_{12}O_{19}$ phase as the major phase.

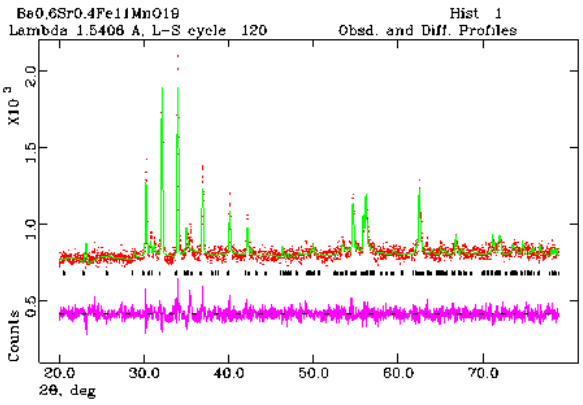

Figure 2 The refinement of the XRD profile of $Ba_{0.6}Sr_{0.4}Fe_{12-z}Mn_zO_{19}$ for z = 1.

Figure 2 shows the refinement result of the diffraction profile of $Ba_{0.6}Sr_{0.4}Fe_{12-z}Mn_zO_{19}$ for z = 1.

The resulting profile shows that there was virtually no residue between the intensity of the observation and calculation results in the entire range of the diffraction angle. The quality factors of fitting, R (criteria of fit) and χ^2 (goodness of fit), were considered acceptable (the χ^2 is less than 1.3) so that the profile has good agreement between observation and calculation. Refinement of the X-ray diffraction pattern confirmed that the $Ba_{0.6}Sr_{0.4}Fe_{12-z}Mn_zO_{19}$ (z = 1) is a single-phase material with a hexagonal structure, with the P 63/m m c space group (194). The structure parameter for the $Ba_{0.6}Sr_{0.4}Fe_{12-z}Mn_zO_{19}$ (z = 1) is summarized in Table 1.

Table 1 Structure Parameter, R Factor, and Goodness of Fit (χ^2).

$Ba_{0.6}Sr_{0.4}Fe_{12-z}Mn_zO_{19}$ (z = 1)		
Space group: P 63/m m c (194), crystal system: hexagonal $a = b = 5.9587(3)$ Å and $c = 23.406(1)$ Å, $\alpha = \beta = 90°$ and $\gamma = 120°$, $V = 719.7(1)$ Å^3 and $\rho = 5.568$ gr.cm^{-3}		
R factor	$\frac{wRp = 3.52}{Rp = 2.72}$	χ^2 (chi-squared) = 1.042

Further confirmation was done by measuring the elemental analysis and observation of the surface morphology of the sample to determine particle distribution, homogeneity and chemical composition using SEM-EDS equipment.

The elemental analysis on the $Ba_{0.6}Sr_{0.4}Fe_{12-z}Mn_zO_{19}$ (z = 1) showed that the sample was well established, as shown in Figure 3.

The microstructure analyses showed that the particle shapes were aggregates with various particle sizes, uniform and evenly distributed on the surface of the sample. The next step was to analyze the element content in the sample using energy dispersive spectroscopy. The details of the elements in the $Ba_{0.6}Sr_{0.4}Fe_{12-z}Mn_zO_{19}$ (z = 1) are shown in Table 2.

Table 2 Results of element analysis using EDS.

No.	**Elements**	**Content**		
		(wt.%)	**(at.%)**	**Stochiometry (at.%)**
1.	Barium (Ba)	7.98 ± 0.41	1.78	1.88
2.	Strontium (Sr)	2.24 ± 0.35	0.78	1.25
3.	Iron (Fe)	49.98 ± 0.32	27.40	34.38
4.	Manganese (Mn)	8.16 ± 0.31	4.55	3.13
5.	Oxygen (O)	31.63 ± 0.13	65.49	59.38

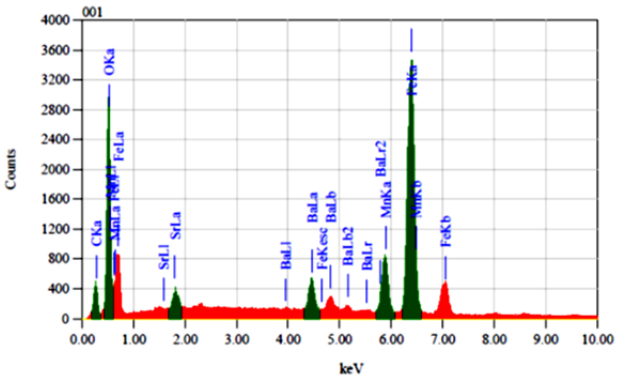

(a)

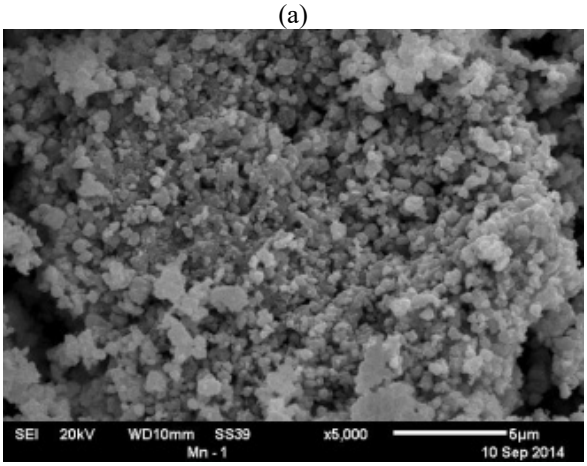

(b)

Figure 3 Elemental analysis and surface morphology of the $Ba_{0.6}Sr_{0.4}Fe_{12-z}Mn_zO_{19}$ (z = 1) sample.

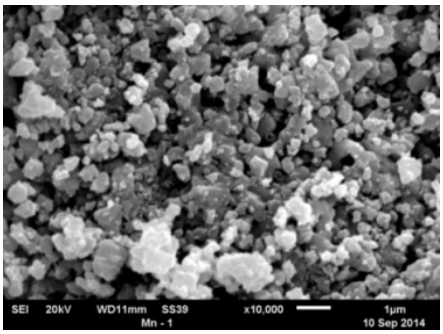

(a)

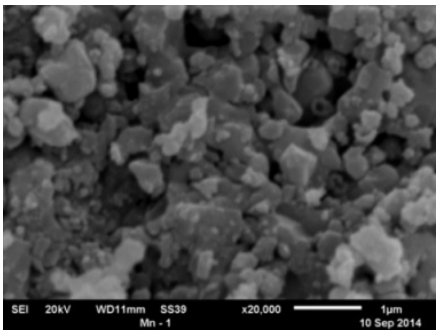

(b)

Figure 4 SEM photographs of Ba0.6Sr0.4Fe12-zMnzO19 (z = 1) particles at (a) 10,000x magnification and (b) 20,000x magnification.

The energy dispersive spectroscopy (EDS) spectra show that the sample had a composition in accordance with the stochiometry parameters. A SEM photograph of the $Ba_{0.6}Sr_{0.4}Fe_{12-z}Mn_zO_{19}$ (z = 1) particles is shown in Figure 4.

The SEM images reveal the morphology of the particles as an aggregate of fine grains. Thus, there is no doubt that this process is adequate in reducing the particle size, changing the particle shape, and improving the particle size distribution. The average particle size estimated from the SEM micrographs in Figure 4 is around ~200-900 nm.

The diffraction profiles for z > 1 were multi-phase. The refinement results of the diffraction profiles of $Ba_{0.6}Sr_{0.4}Fe_{12-z}Mn_zO_{19}$ (z > 1) are shown in Table 3.

Table 3 Mass fraction of $Ba_{0.6}Sr_{0.4}Fe_{12-z}Mn_zO_{19}$ (z = 0, 1, 2, and 3).

z	Sample	Mass fraction	
		Phase	**(wt.%)**
0	$Ba_{0.6}Sr_{0.4}Fe_{12}O_{19}$	$BaFe_{12}O_{19}$	100
1	$Ba_{0.6}Sr_{0.4}Fe_{11}MnO_{19}$	$BaFe_{12}O_{19}$	100
2	$Ba_{0.6}Sr_{0.4}Fe_{10}Mn_2O_{19}$	$BaFe_{12}O_{19}$	92.53 ± 0.06
		Mn_2O_3	7.47 ± 0.01
3	$Ba_{0.6}Sr_{0.4}Fe_9Mn_3O_{19}$	$BaFe_{12}O_{19}$	81.40 ± 0.02
		SrO	2.79 ± 0.06
		Fe_2O_3	2.62 ± 0.01
		Mn_2O_3	13.19 ± 0.01

The typical particle size distribution for the $Ba_{0.6}Sr_{0.4}Fe_{12-z}Mn_zO_{19}$ (z = 1) sample is shown in Figure 5. The mono modal curves for the sample indicate that the particles suspended in the dispersant media were homogeneous. However, the particles of the $Ba_{0.6}Sr_{0.4}Fe_{12-z}Mn_zO_{19}$ (z = 1) powder showed a narrower particle size distribution with a mean particle size of ~850 nm.

The phase identification refers to the research results of Zlatkov, *et al.* [9], Rutt, *et al*. [10], Al-Saie, *et* al. [11], and Jankovskýa, *et al.* [12] for the phase of barium hexa-ferrite ($BaFe_{12}O_{19}$), strontium oxide (SrO), hematite (Fe_2O_3), and manganese oxide (Mn_2O_3), respectively. The refinement result, revealed that manganese substitution in the iron atoms was only able to reach the limit of z = 1. A doping concentration of z > 1 formed another phase.

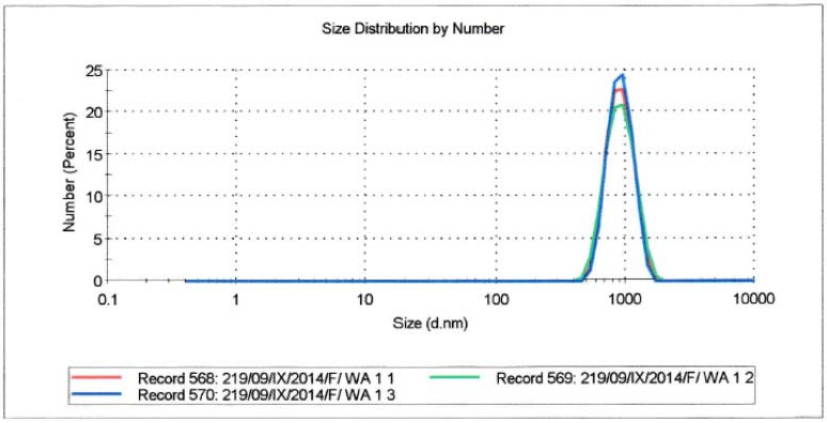

(a)

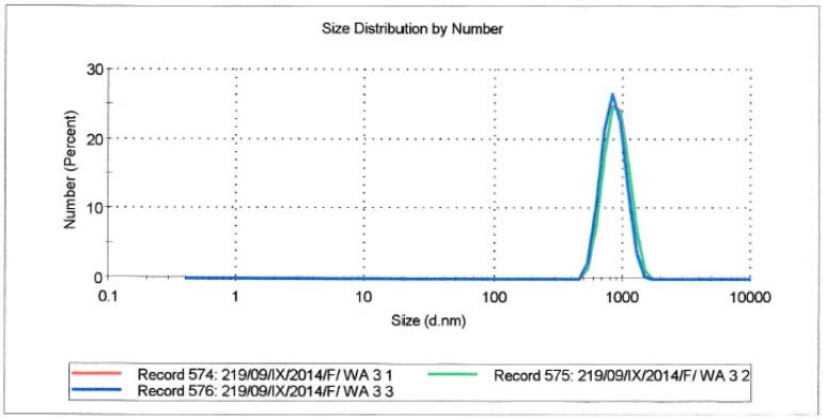

(b)

Figure 5 Particle size distribution of the $Ba_{0.6}Sr_{0.4}Fe_{12-z}Mn_zO_{19}$ (z = 1) sample at (a) PSA-1 and (b) PSA-2.

3.2 Magnetic and Microwave Absorbing Properties

Characterization of the magnetic properties of the $Ba_{0.6}Sr_{0.4}Fe_{12-z}Mn_zO_{19}$ (z = 0, 1, 2, and 3) magnetic particles was performed using a vibrating sample magnetometer (VSM) that produces hysteresis curves of magnetic particles.

The hysteresis curves of the synthesized $Ba_{0.6}Sr_{0.4}Fe_{12-z}Mn_zO_{19}$ are shown in Figure 6, in which the respective profiles for z of 0, 1, 2, and 3 are also compared. The hysteresis loop as shown in Figure 6 was characterized with intrinsic saturation Ms, remanence field Mr, and coercivity Hc. The intrinsic saturation, is the state when the material is not able to absorb any more magnetic fields, so increasing the magnetization force will not significantly change the magnetic flux density. Meanwhile, the remanence field, is the

residual magnetization in a medium once the external magnetic field is removed. Coercivity (also called coercive force) is the force required to demagnetize the material so residual induction becomes zero after magnetizing up to saturation. The hysteresis loops in Figure 7 for $Ba_{0.6}Sr_{0.4}Fe_{12-z}Mn_zO_{19}$ (z = 0, 1, 2, and 3) show the magnetic data, which are summarized in Table 4.

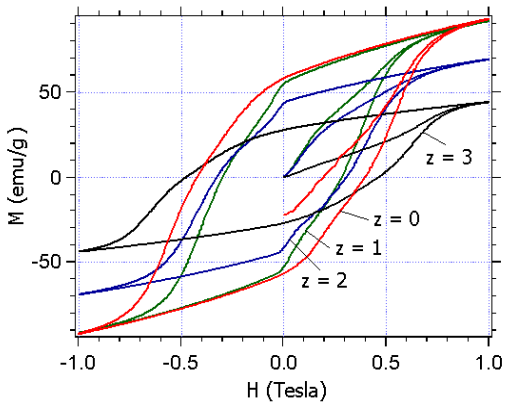

Figure 6 The hysteresis curves of $Ba_{0.6}Sr_{0.4}Fe_{12-z}Mn_zO_{19}$ (z = 0, 1, 2, and 3).

Table 4 Summary of magnetization measurement for samples.

z	Hc (T)	Ms (emu/gr)	Mr (emu/gr)
0	0.424	92.9	58.0
1	0.299	92.0	54.9
2	0.328	69.2	43.3
3	0.478	44.2	27.9

Based on the hysteresis curves, the magnetic moment of the $Ba_{0.6}Sr_{0.4}Fe_{12-z}Mn_zO_{19}$ (z = 0, 1, 2, and 3) magnetic particles can be determined. The magnetic moments of the $Ba_{0.6}Sr_{0.4}Fe_{12-z}Mn_zO_{19}$ (z = 0, 1, 2, and 3) magnetic particles that were generated, were 92.9, 92.0, 69.2, and 44.2 emu/gr respectively. The magnetic properties of the $Ba_{0.6}Sr_{0.4}Fe_{12-z}Mn_zO_{19}$ (z = 1) particles showed a low coercivity and a high remnant magnetization of 54.9 emu/gr. While the Ba0 $Ba_{0.6}Sr_{0.4}Fe_{12-z}Mn_zO_{19}$ (z = 1) particles show a high coercivity and a low remnant magnetization, it is considered a hard magnetic material. Such materials are typically called permanent magnets. The decreased coercivity value (z = 1) is likely due to the iron successfully being substituted by manganese atoms. This condition is actually necessary in order for the magnetic spin to more easily resonate with the microwaves and hence this material is useful as a microwave absorber. The decreased value of magnetization (z > 1) was likely due to the added manganese not successfully substituting iron atoms, so the fraction of magnetism decreased.

The microwave absorbing properties of the synthesized $Ba_{0.6}Sr_{0.4}Fe_{12-z}Mn_zO_{19}$ are shown in Figure 7 in which the respective profiles for z of 0, 1, 2, and 3 are also compared. According to the theory of electromagnetic radiation, the reflection loss, RL (dB), can be defined as

$$RL(dB) = 20 \log \left| \frac{Zin - Zo}{Zin + Zo} \right|.$$

Figure 7 shows the relation between the reflection loss (RL) of the $Ba_{0.6}Sr_{0.4}Fe_{12-z}Mn_zO_{19}$ (z = 0, 1, 2, and 3) and the microwave frequency X-band in the range of 8-14 GHz when the thickness of the sample is 1.5 mm. At least two absorption peaks with a high RL within the frequency range can be observed for all samples.

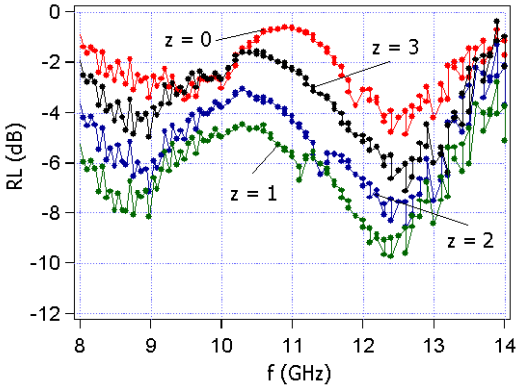

Figure 7 The reflection loss (RL) curves of $Ba_{0.6}Sr_{0.4}Fe_{12-z}Mn_zO_{19}$ (z = 0, 1, 2, and 3).

The phase composition showed in the Figure 7, shows that the $Ba_{0.6}Sr_{0.4}Fe_{12-z}Mn_zO_{19}$ (z = 0) has a low RL, which increases for z = 1 and decreases again for z = 2 and 3. This case shows that even though the best absorber for Mn substituted Ba-Sr hexaferrite for z = 0, 1, 2, and 3 occurred at nearly the same thickness and at practically identical frequencies, there were differences. This can be explained by the effect of the electromagnetic properties on the attenuation characteristic of each sample. It was found that substitution with Mn effectively increased the attenuation constant in the entire range of frequencies used here, compared with non-substitution (z = 0). The optimum value of microwave absorption was found on the phase composition of z = 1. There are two important conditions to be fulfilled for the material to have high absorption of electromagnetic waves. The first is called characteristic impedance matching. The intrinsic impedance of the material must be equal to the intrinsic impedance of free space. The second is the interaction between the electromagnetic energy

and the material, which must be able to weaken the incoming electromagnetic waves. This means that the material behaves both as a dielectric and a magnetic material. Therefore, some intrinsic properties of the magnetic phase anisotropy constants governing the coercivity value should be reduced. One way to decrease this significantly is by substituting Mn on the barium hexaferrite. This relates to a change in the Fe^{3+} magnetic moments after they are substituted by Mn^{2+}. This indicates that $Ba_{0.6}Sr_{0.4}Fe_{12-z}Mn_zO_{19}$ (z = 1) has certain microwave absorption properties in the frequency range of 8-14 GHz, with absorption peak values of -8 dB at 8.5 GHz and -10.0 dB at 12.5 GHz.

4 Conclusions

Synthesis of $Ba_{0.6}Sr_{0.4}Fe_{12-z}Mn_zO_{19}$ (z = 0, 1, 2, and 3) was successfully performed by solid state reaction through a mechanical milling method. It was found that the best phase composition with a high performance absorber was $Ba_{0.6}Sr_{0.4}Fe_{11}MnO_{19}$. Refinement of the X-ray diffraction patterns showed that the $Ba_{0.6}Sr_{0.4}Fe_{11}MnO_{19}$ was single-phase, with a hexagonal structure (P 63/m m c) and the values of *a*, *b* and *c* were 5.9587(3) Å, 5.9587(3) Å and 23.406(1) Å, respectively. The hexagonal structure had an angle of $\alpha = \beta = 90°$ and $\gamma = 120°$, and its volume and density were found to be 719.7(1) $Å^3$ and 5.568 $gr.cm^{-3}$, respectively. The mechanical milling of $Ba_{0.6}Sr_{0.4}Fe_{11}MnO_{19}$ powders produced particles with a mean size of ~850 nm. SEM imagery revealed the morphology of the particles as being aggregates of fine grains. The magnetic properties of the $Ba_{0.6}Sr_{0.}4Fe_{11}MnO_{19}$ particles showed a low coercivity and a high remanent magnetization. Moreover, the $Ba_{0.6}Sr_{0.4}Fe_{11}MnO_{19}$ had certain microwave absorber properties in the frequency range of 8-14 GHz, with absorbing peak values of -8 dB and -10 dB at frequencies of 8.5 and 12.5 GHz, respectively.

Acknowledgements

This work was supported by DIKTI Competitive Grants 2014 No. DIPA: SP DIPA-023.04.2.189705/2014, The Development of Magnetic Materials based Composite Systems $(Ba_{(1-y)}Sr_y)O.6Fe_{2(1-x)}(Mn,Ti)_xO_3$ for Interference Absorption of Electromagnetic Waves on Cell Phones.

References

[1] Mustofa, A, Mardiana, H., Noor, B.I. & Nazlim, Y.A., *Microwave Magnetic Dielectric Properties of Some Cerium Ytrium Garnet*, J. Sains Malaysia, **37**, pp. 202-210, 2008.

[2] Li, Z.W., Guoqing, L., Linfeng, C., Wu, Y. & C.K., Ong, *Co^{2+} Ti^{4+} Substituted Z-type Barium Ferrite with Enhanced Imaginary Permeability*

and Resonance Frequency, J. of App. Phys., **99**(6), pp. 063905-063905-7, 2006.

[3] Zhang, H., Yao, X., Wu, M. & Zhang, L., *Complex Permitivity and Pearmibility of Zn-Co Substituted Z-type Hexaferrite Prepared by Citrate Sol-gel Process*, British Cer. Transc., **102**, pp. 1-10, 2003.

[4] González-Angeles, A., Grusková, A., Lipka, J., Sláma, J. & Jančárik, V., *Magnetic and Structural Studies of $Ba_{0.5}Sr_{0.5}(ZnTi)_xFe_{12-2x}O_{19}$ Prepared by Ball Milling*, Jordan Journal of Phys., **1**(1), pp. 37-42, 2008.

[5] Shams, M.H., Salehi, S.M.A. & Ghasemi, A., *Electromagnetic Wave Absorption Characteristics of Mg–Ti Substituted Ba-hexaferrite*, Materials Letters, **62**, pp. 1731-1733, 2008.

[6] Li, X.C., Gong, R., Feng, Z., Yan, J., Shen, X. & He, H., *Effect of Particle Size and Concentration on Microwave-Absorbing Properties of Hexaferrite Composites*, J. Am. Ceram. Soc., **89**(4), pp. 1450-1452, 2006.

[7] Qiu, J., Shen, H. & Gu, M., *Microwave Absorption of Nanosized Barium Ferrite Particles Prepared using High-energy Ball Milling*, Powder Technology, **154**, pp. 116-119, 2005.

[8] Toby, B.H., *EXPGUI*, *A Graphical User Interface for GSAS*, Journal of Applied Crystallography, **34**, pp. 210-213. 2001.

[9] Zlatkov, B.S. Nikolic, M.V., Aleksic, O., Danninger, H. & Halwax, E., *A Study of Magneto-crystalline Alignment in Sintered Barium Hexaferrite Fabricated by Powder Injection Molding*, Journal of Magnetism and Magnetic Materials, **321**, pp. 330-335. 2009.

[10] Rutt, O.J., Williams, G.R. & Clarke, S.J., *Reversible Lithium Insertion and Copper Extrusion in Layered Oxysulfides*, Chemical Communications, **27**, 2006.

[11] Al-Saie, A.M., Al-Shater, A., Arekat, S., Jaffar, A. & Bououdina, M., *Effect of Annealing on the Structure and Magnetic Properties of Mechanically Milled TiO_2–Fe_2O_3 Mixture*, Ceramics International, **39**(4), pp. 3803-3808, 2013.

[12] Jankovskýa, O., Sedmidubskýa, D., Šimeka, P., Sofera, Z., Ulbrich, P. & Bartůněka, V., *Synthesis of MnO, Mn_2O_3 and Mn_3O_4 Nanocrystal Clusters by Thermal Decomposition of Manganese Glycerolate*, Ceramics International, **41**(1), Part A, pp. 595-601, 2015.